Electronic Supplementary Information:

Unravelling the Key Role of Ion-Exchange Membranes in Water Management and Ion Crossover for Zero-Gap CO₂ Electrolyzers

Lieven Hintjens[a], Sam Van Daele[a], Jonathan Schalck[a], Michiel Vranckaert[a], Sander Neukermans[a], Daniel Choukroun[a], Tom Breugelmans[a,*]

[a] Applied Electrochemistry and Catalysis (ELCAT), University of Antwerp, 2610 Wilrijk, Belgium

* Corresponding author – Tom.Breugelmans@uantwerpen.be

Section 1: Electrolyzer design

In Figure S1 below, the electrolyzer design used in this study is displayed with individual designation of all components. The complete setup, including pumps and mass-flow controller (MFC) is visualized in Figure S2.

Figure S1 Overview electrolyzer design with all components: (1) aluminium front- and backplate; (2) PMMA insulation plate; (3) copper current collector; (4) graphite cathode flowplate with interdigitated flow pattern (7 cm x 7 cm); (5) PTFE gasket with 39BB GDE covered with catalyst (SnO_2 or Bi_2O_3); (6) Nafion® cation exchange membrane (N117 or N211); (7) PTFE gasket with nickel foam; (8) graphite anode flowplate with interdigitated flow pattern.
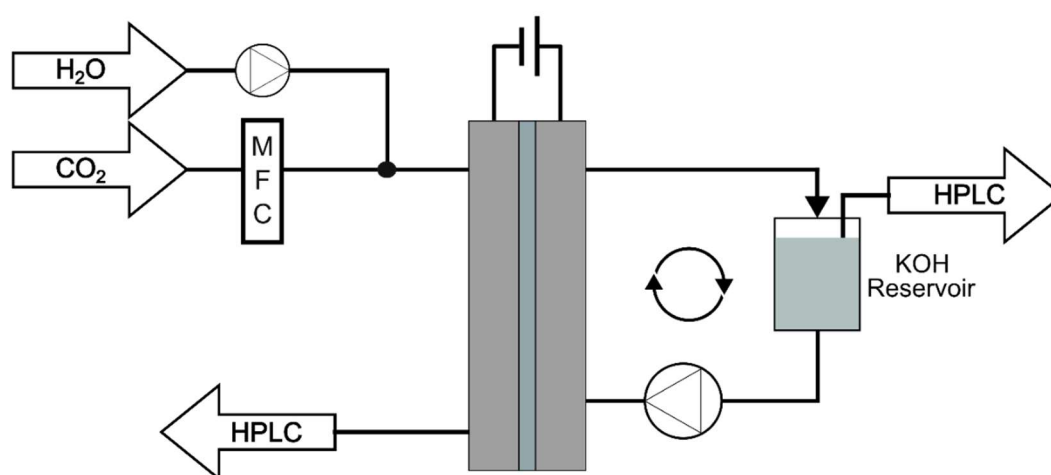

Figure S2 Process flow diagram of the CO_2 reduction setup. The CO_2 flow rate (612 sccm) is controlled via a mass flow controller (MFC), after which water is mixed (0.65 ml/min) via direct water injection (DWI). The anolyte (KOH-solution – $C_{initial}$ = 1.7 M) is recirculated by a membrane pump at a flow rate of 100 ml/min for efficient gas bubble removal.

Section 2: Correlation cell voltage – re-oxidation

In the figures below, the cell voltages is plotted vs time. Due to the absence of a reference electrode in the zero-gap electrolyzer, the changes in voltage cannot only be ascribed to the cathode, but also to other components in the system. Often a low reproducibility in cell voltage is observed mainly due the influence of: corrosion of the copper current collectors, degradation of Ni-foam or slight differences in electrolyzer compression.

However, concerning the reoxidation of formate, a clear correlation can be identified. When the reoxidation of formate is initiated, indicated by the deviation of the accumulated formate (green curve) from the linear increase, a significant rise in cell voltage occurs. This increase in accumulated formate is a result of the constant crossover to the recirculated anolyte.
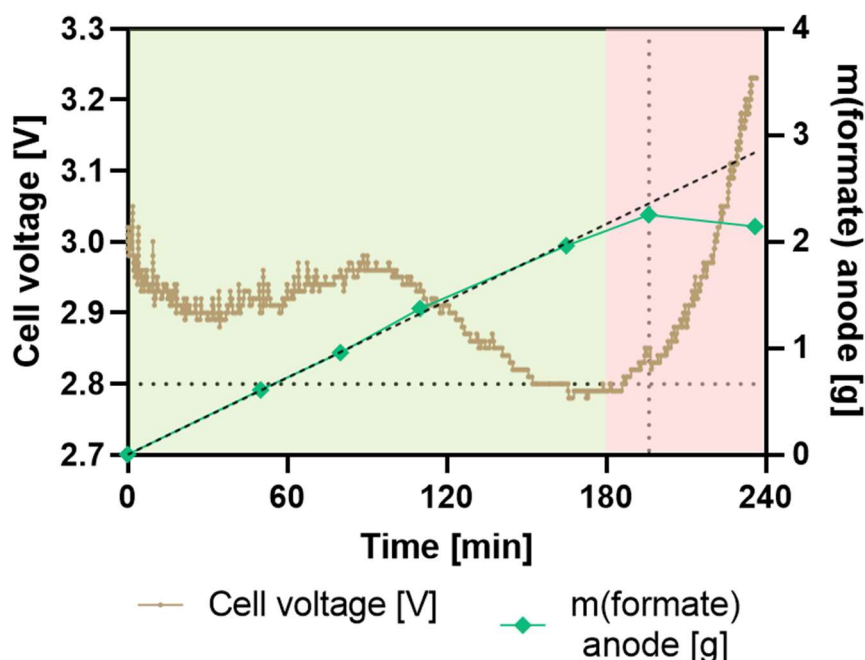

Figure S3 Correlation between cell voltage and formate re-oxidation for an N117 membrane under galvanostatic operation (100 mA/cm²). An anolyte with an initial concentration of 1.7 M KOH and initial volume of 500 ml was utilized.
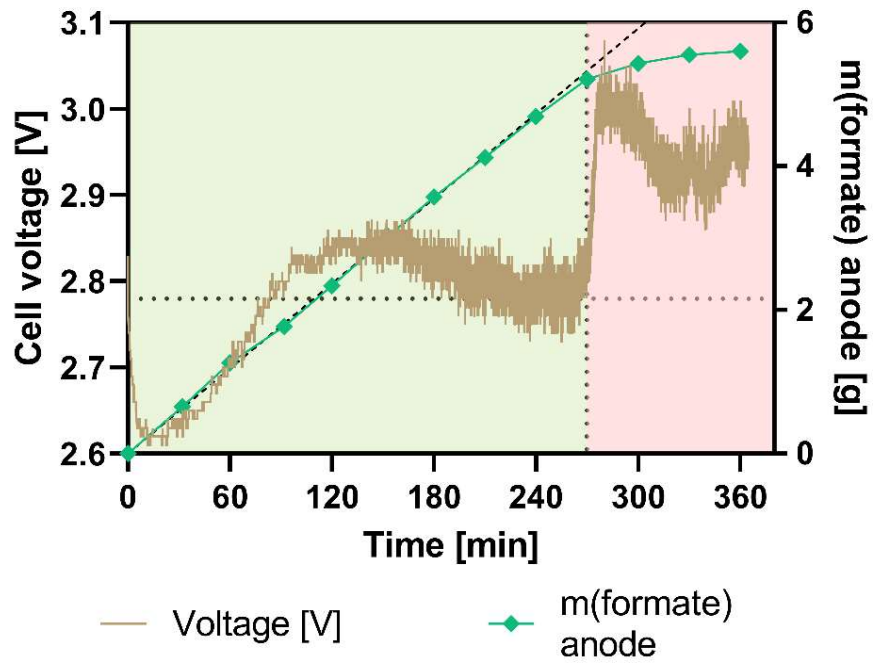
Figure S4 Correlation between cell voltage and formate oxidation for an N211 membrane under galvanostatic operation (100 mA/cm²). An anolyte with an initial concentration of 1.7 M KOH and initial volume of 1000 ml was utilized.

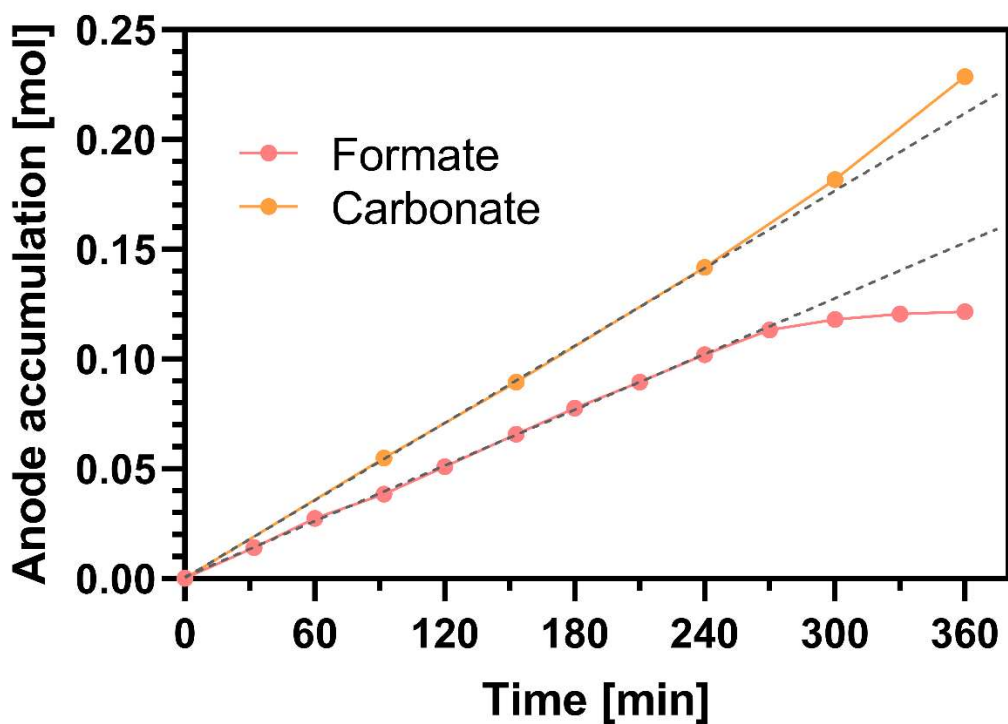# Section 3: Correlation anode carbonate concentration – formate re-oxidation

Figure S5 Accumulation of carbonates and formate in the anode compartment (V = 1000 ml) as a result of crossover from the cathode to the anode compartment. The amount of carbonates is measured by TIC-analysis, while the formate concentration is measured by HPLC.

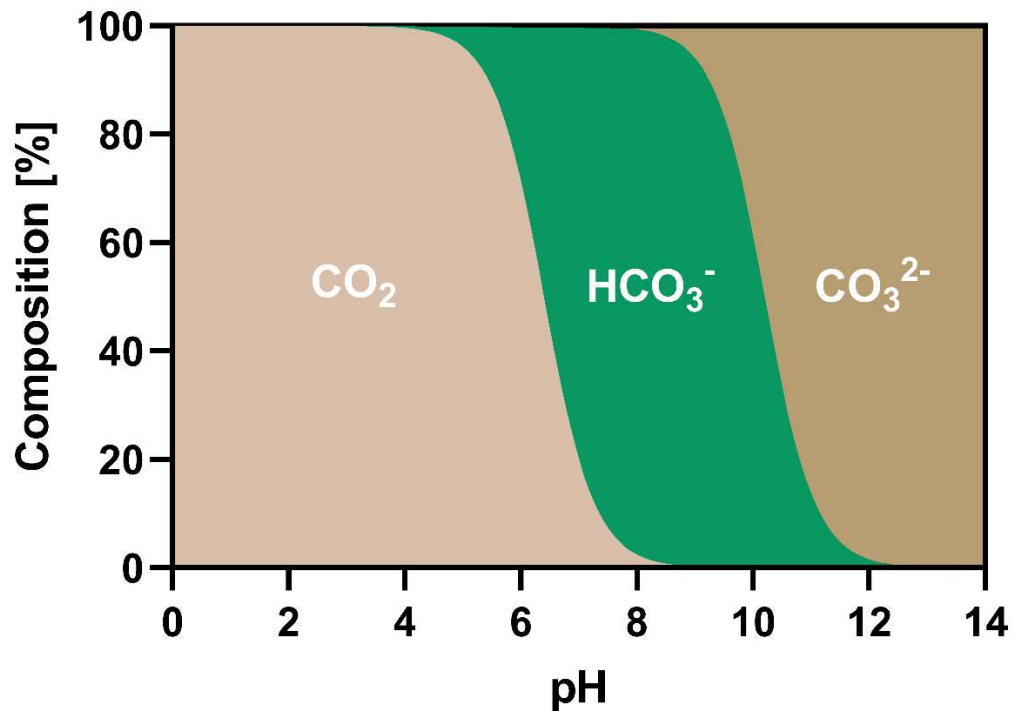# Section 4: Carbon dioxide – bicarbonate – carbonate equilibrium

Figure S6 Carbon dioxide - bicarbonate – carbonate equilibrium for different pH values.

$$\% CO_2 = \frac{1}{\frac{K_{a1}}{10^{-pH}} + 1} \times 100$$

$$\% HCO_3^{-} = \frac{1}{\frac{10^{-pH}}{K_{a1}} + \frac{K_{a2}}{10^{-pH}} + 1} \times 100$$

$$\% CO_3^{2-} = \frac{1}{\frac{10^{-pH}}{K_{a2}} + 1} \times 100$$

With $K_{a,1} = 3.98 \cdot 10^{-7}$ and $K_{a,2} = 6.31 \cdot 10^{-1}$ [1]

Section 5: Calculation methods

5.1. Minimum water supply

Since $KHCO_3$ has the lowest solubility and is thus most prone to precipitation, its formation rate determines the minimum water supply. The production rate of $KHCO_3$ is determined by TIC-analysis. Secondly, the water which is consumed by the CO2RR and HER also needs to be taken into account.

$$\varphi_{H2O,min} = \varphi_{H2O,salt} + \varphi_{H2O,react}$$

With φ_{H2O} = supply rate of water [ml/min]

$$\varphi_{H2O,min} = \frac{\dot{n}_{HCO3}}{S(KHCO_3)} + \frac{I}{F} * 60 * \left(\frac{FE_{HCOO-}}{2*100} + \frac{FE_{H2}}{1*100}\right) * \frac{M_{H2O}}{\rho_{H2O}}$$

With $\dot{n}_{HCO3}$ = production rate of bicarbonates [mmol/min]

$S(KHCO_3)$ = solubility of $KHCO_3$ in water [mmol/ml]

and I = current [A]

F = Faraday constant [96 485 C/mol]

FE_i = Faradaic efficiency component i [%]

M_i = molar mass component i [g/mol]

ρ_i = density of component i [g/ml]

5.2. Hydroxide-associated flux

The principle of electroneutrality inside an electrolyzer states that the total charge transferred by ions has to be identical to the charge transferred by electrons: [2]

$$\sum I_i = 0$$

$$I_{ext} - I_{K^+} + I_{HCOO^-} + I_{OH^-} = 0$$

With I_{ext} is the external current, I_K the potassium associated current, I_{HCOO} the formate associated current and I_{OH} the hydroxide associated current, with counter-clockwise flow considered as positive.

Above equation can be transformed to:

$$I_{ext} = (J \cdot A_m \cdot z \cdot F)_{K^+} - (J \cdot A_m \cdot z \cdot F)_{HCOO^-} - (J \cdot A_m \cdot z \cdot F)_{OH^-}$$

$$\Leftrightarrow \frac{I_{ext}}{F \cdot A_m} = J_{K^+} \cdot (+1) - J_{HCOO^-} \cdot (-1) - J_{OH^-} \cdot (-1)$$

$$\Leftrightarrow \frac{I_{ext}}{F \cdot A_m} = J_{K^+} + J_{HCOO^-} + J_{OH^-}$$

$$\Leftrightarrow J_{OH^-} = \frac{I_{ext}}{F \cdot A_m} - J_{K^+} - J_{HCOO^-}$$

With J_i is the flux of ion i across the membrane ($mol/(cm^2\ s)$), A_m the membrane exchange area (cm^2), z_i is the charge of ion i and F the Faraday constant (96 485 C/mol).

5.3. Humidity CO_2 feed

Following Dalton's law and ideal gas behaviour:

$$p_{H2O} = x_{H2O} \cdot p_{total}$$

$$x_{H2O} = \frac{p_{H2O}}{p_{total}} = \frac{p_{H2O}^{\circ}}{p_{total}} = \frac{3170\ Pa}{101325\ Pa} = 0.031$$

$$\text{with } p_{H2O}^{\circ}(25°C) = 3170\ Pa \quad [3]$$

At saturation, the water(vapor) reaches a concentration of 3.1 mol% water.

Following the Ideal Gas law, the (molar) gas flow can be calculated:

$$\dot{n} = \frac{p \cdot \dot{V}}{R \cdot T} = \frac{101325\ Pa \cdot (0.612 \cdot 10^{-3}\ m^3/min)}{8.314\ {}^{J}/_{mol \cdot K} \cdot 298\ K} = 2.5 \cdot 10^{-2}\ mol\ gas/min$$

The molar flow of water can be calculated:

$$\dot{n}_{H2O} = x_{H2O} \cdot \dot{n}_{total} = 0.031 \cdot 2.5 \cdot 10^{-2}\ mol\frac{gas}{min} = 7.8 \cdot 10^{-4}\ mol\ H_2O/min$$

$$\dot{m}_{H2O} = \dot{n}_{H2O} \cdot M_{H2O} = 7.8 \cdot 10^{-4}\ \frac{mol\ H_2O}{min} \cdot 18\ \frac{g}{mol} = 1.41 \cdot 10^{-2}\frac{g\ H_2O}{min}$$

$$\dot{V}_{H2O} = \frac{\dot{m}_{H2O}}{\rho_{H2O}} = \frac{1.41 \cdot 10^{-2}\frac{g}{min}}{0.997\frac{g}{ml}} = 0.014\ ml/min$$

Since a supply of 0.65 ml/min water is fed, it is assumed the CO_2 stream is oversaturated.

Since the vapor pressure increases with the temperature, the supply of water vapor increases when preheating the CO_2 gas as indicated in Figure S7 below:
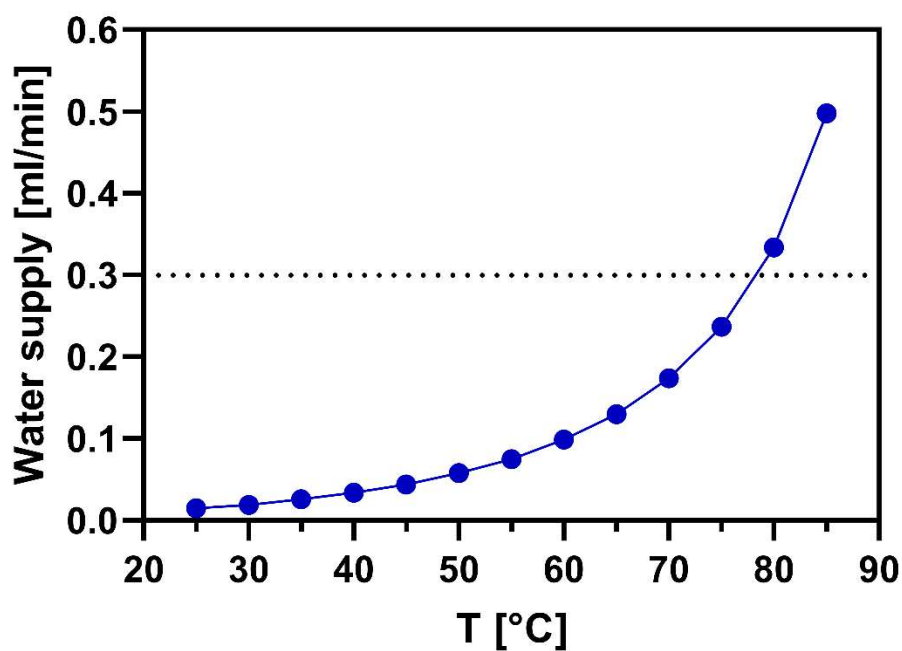
Figure S7 Influence of temperature on the water vapor supply, for a saturated gas. The dotted line indicates the minimum water supply (0.3 ml/min – 4.9 A) for the CO2RR to occur and to remove the produced carbonate salts.

To supply the minimum water amount of 0.3 ml/min (at 100 mA/cm² and 49 cm²), a minimum inlet temperature of 78.5°C is required. However, to dissolve the salts the water should be present in the liquid form and this approach assumes that all the water vapor condenses at the catalytic active area, which is unlikely. Therefore the CO_2/water mixture should be supplied at a higher temperature than 78.5°C, assuming an electrode at standard temperature.

5.4. Membrane permeation

Since the formed products (HCOOK, CO, H_2, $KHCO_3$, K_2CO_3) are either solid or gaseous (no liquids are formed), membrane permeation can be estimated based on the flow rate of the outgoing cathode product.

$$MP = CF - DWI + RW$$

With MP = membrane permeation [ml/min]

CF = Cathode product flow rate [ml/min]

DWI = Direct water injection flow rate [ml/min]

RW = Water consumed by CO2RR/HER reaction [ml/min]

$$RW = \frac{FE(HCOO^-)}{100} \cdot \frac{M(H_2O)}{2} \cdot \frac{I \cdot 60}{F} + \frac{FE(H_2)}{100} \cdot \frac{M(H_2O)}{1} \cdot \frac{I \cdot 60}{F}$$

With $M(H_2O)$ = molar mass water [18.015 g/mol]

F = Faraday constant [96 485 C/mol]

I = Current [A]

FE(i) = Faradaic efficiency of component i [%]

Section 6: Influence of DWI flow rate on CO2RR stability

Throughout this manuscript, a DWI-flow rate of 0.65 ml/min was injected into the CO_2 stream (ESI – Section 5.3). To improve the water supply (and thus salt removal) while using a low permeating membrane (0.15 - 0.2 ml/min), a higher DWI-flow rate of 1.00 ml/min vs 0.65 ml/min was tested.
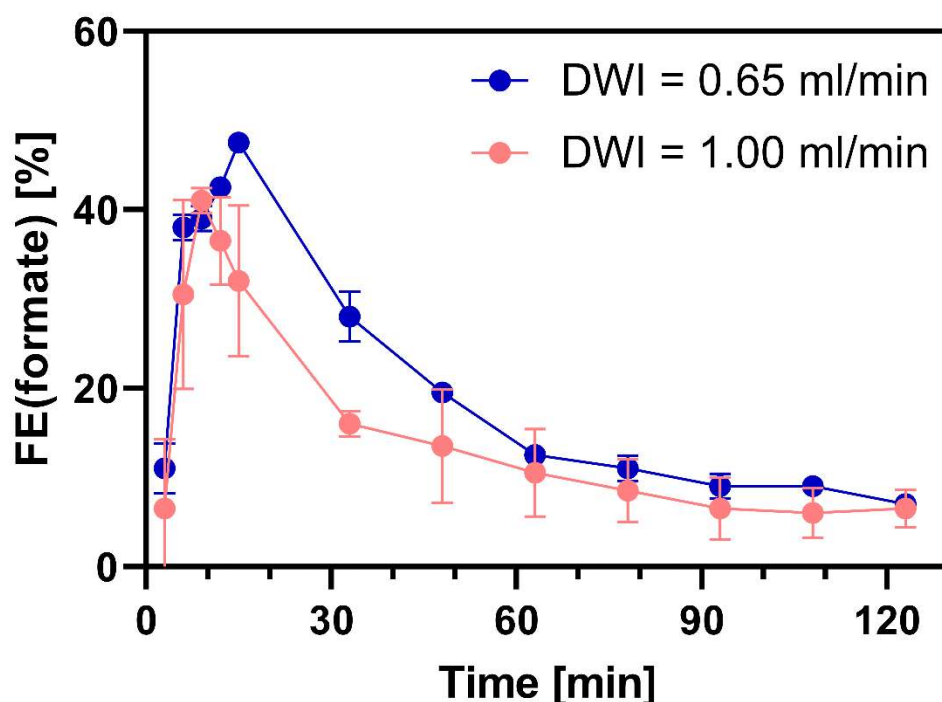

Figure S8 FE(formate, uncorrected) vs time for two direct water injection flow rates: 0.65 ml/min (blue curve) and 1.00 ml/min (red curve) while using a low permeating membrane (N117). Every experiment was carried out twice. Both flow rates were tested under identical process conditions: 100 mA/cm², flow rate CO_2 of 612 sccm and catalyst loading of 4 mg/cm².

These results indicate that a higher DWI flow rate (1.00 ml/min) is less favourable due to lower reproducibility and stability as a result of flooding in the macro-porous layer of the GDE substrate. Even though increasing the DWI-feed above 0.65 ml/min had no positive effect, a minimum DWI was still deemed necessary to prevent salt build-up in the CO_2 flowplate channels when utilizing a low permeating membrane (< 0.2 ml/min).

The effect of decreasing the DWI-flow rate was tested in combination with a high permeating membrane (N211, MP = 0.5 ml/min). As visible in Figure S9, when supplying a DWI-feed of 0.3 ml/min, a similar stability (+6 hours) is achieved compared to operation with a DWI-feed of 0.65 ml/min. Irrespective of the lower DWI supply, the salt management remained adequate with a crystallization of 0.78 ± 0.24 mg/cm². The reduced diluting effect on the cathode product, however, adds the benefit of a higher product concentration of 0.79 ± 0.03 M (vs 0.57 ± 0.02 M), thereby increasing economic value.
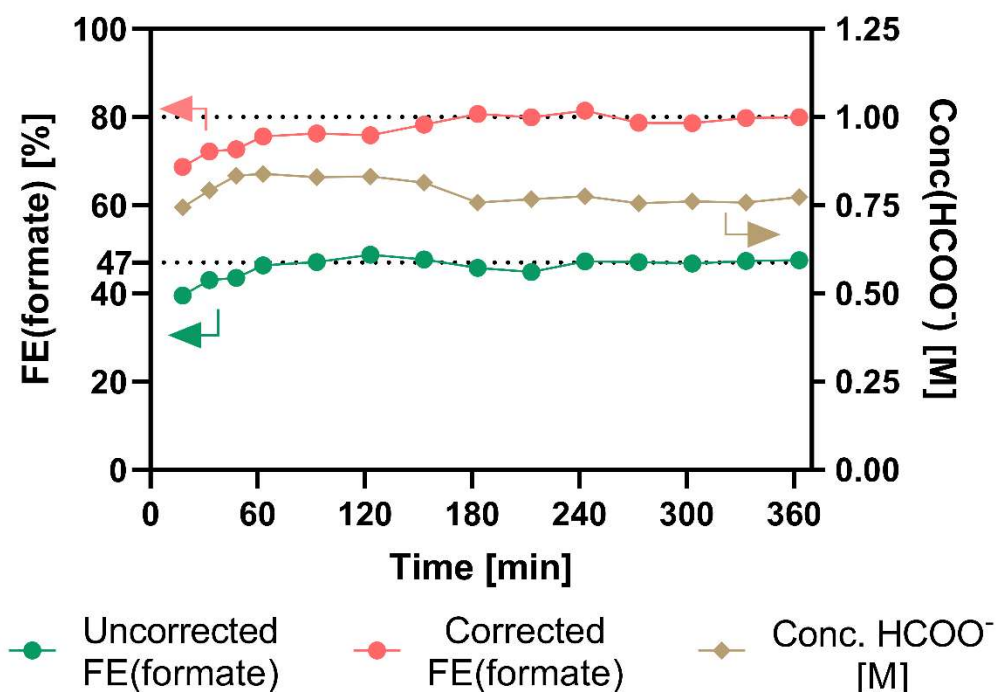

Figure S9 FE(formate) and formate concentration in cathode product vs time when utilizing a DWI-feed of 0.3 ml/min. The electrolyzer is operated at a CD of 100 mA/cm² and SnO₂ as cathode catalyst. To maximize the membrane permeation, a thin N211 membrane is incorporated.

When excluding the DWI completely (no humidification of CO_2 feed) no stable operation of the electrolyzer was deemed possible, as visible in Figure S10, due to salt formation in the cathode flowplate. After one hour of operation, the experiment had to be terminated because of salt buildup at the top of the cathode flowplate, hindering the CO_2 flow from being distributed over the GDE. We attribute this observation to

the elevated pressure in the flowplate header, which impedes water permeation through the membrane in this area, consequently leading to more critical water and salt management.
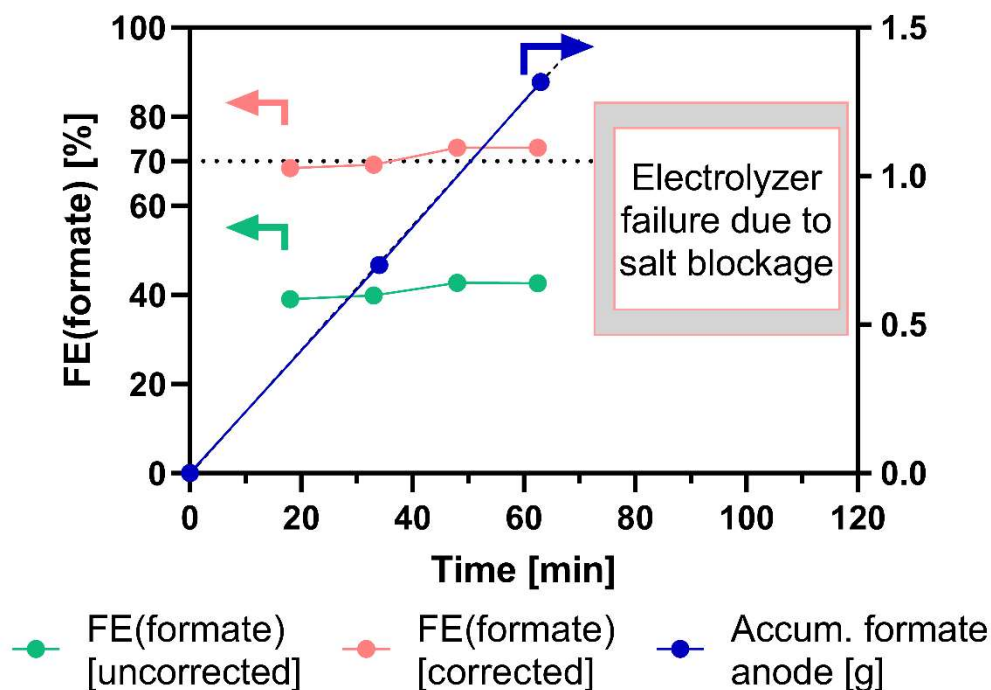

Figure S10 FE(formate) and formate concentration in cathode product vs time without utilizing a DWI. The electrolyzer is operated at a CD of 100 mA/cm² and SnO₂ as cathode catalyst. To maximize the membrane permeation, a thin N211 membrane is incorporated.

Therefore, a minimum DWI-feed is still considered necessary to prevent salt build-up in the cathode flowplate. The DWI flow rate, however, requires further optimization to minimize the diluting effect of the final product.

Section 7: Promoted catalyst degradation: particle detachment

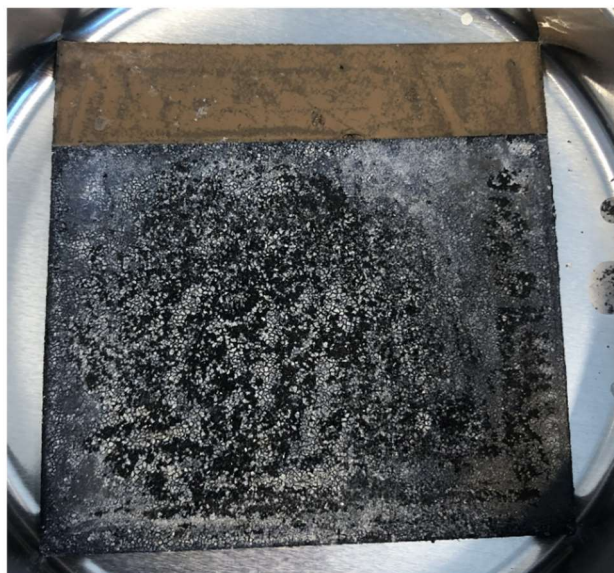<u>Low membrane permeation (0.09 ml/min)</u>

Figure S11 Used GDE (with SnO₂ nanoparticles) subject to catalyst detachment as a result of a low membrane permeation (0.09 ml/min) through a degraded N117 membrane. Without catalyst detachment, a homogeneous grey colour is visible (as depicted in Figure S13). The black spots on this GDE indicate the detachment of catalyst, making the carbon paper below visible.
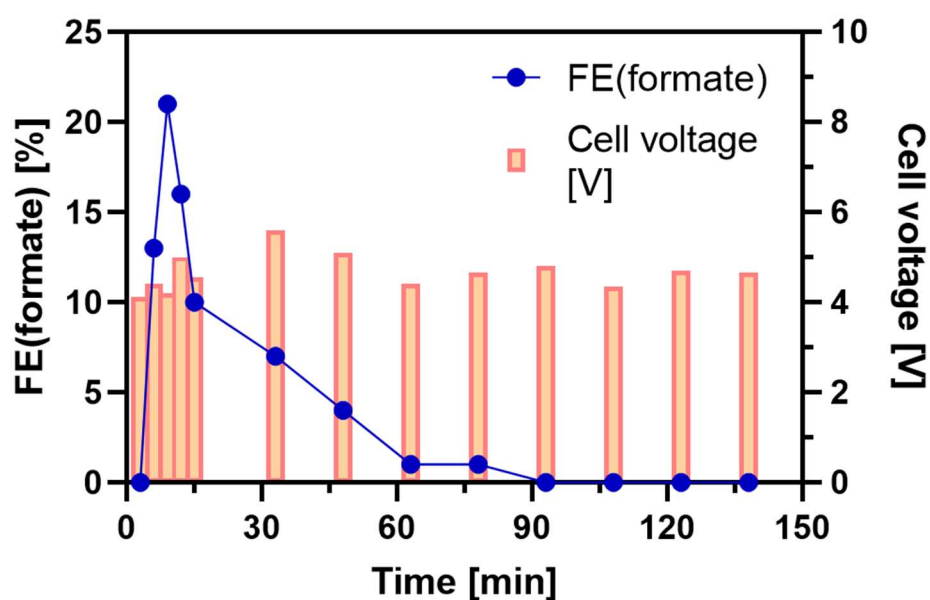

Figure S12 Uncorrected FE(formate) and cell voltage vs time for GDE subject to catalyst detachment (Figure S11) supplied by low membrane permeation (0.09 ml/min) through a degraded N117 membrane. The cell voltage corresponds to a current density of 100 mA/cm².
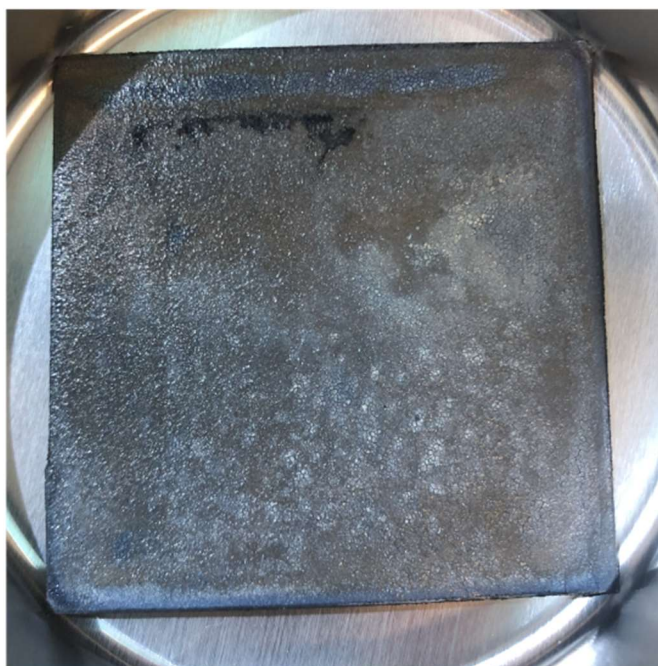
High membrane permeation (0.36 ml/min)

Figure S13 Used GDE covered with a SnO$_2$ catalyst-based layer, in the absence of catalyst detachment and operated under high membrane permeation (0.36 ml/min) conditions through a pristine N117 membrane.
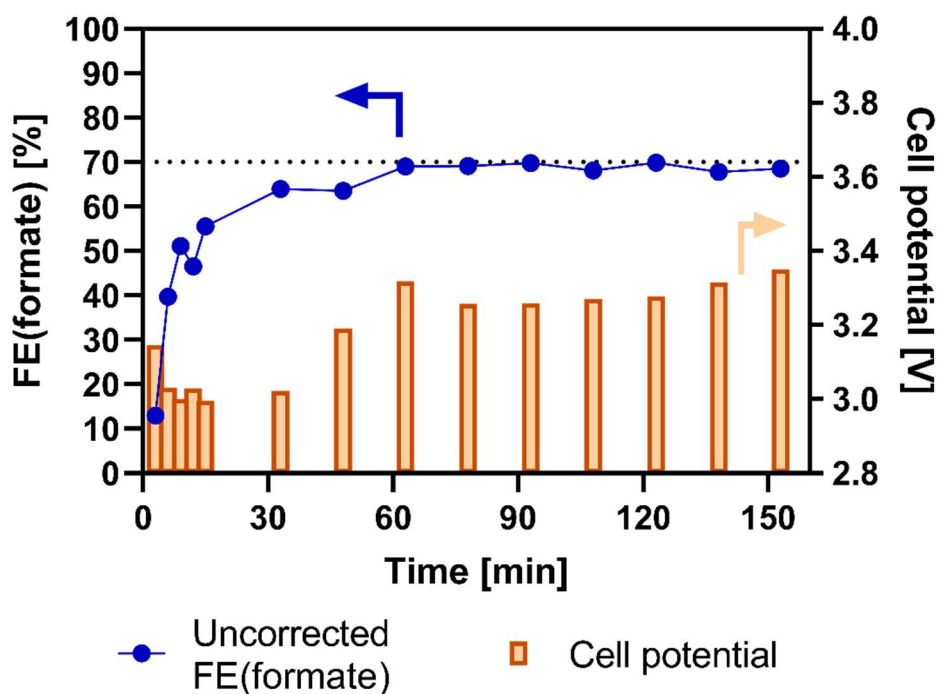

Figure S14 Uncorrected FE(formate) and cell voltage vs time for GDE without catalyst detachment supplied by high membrane permeation (0.36 ml/min) through pristine N117 membrane. The cell voltage corresponds to a current density of 100 mA/cm².

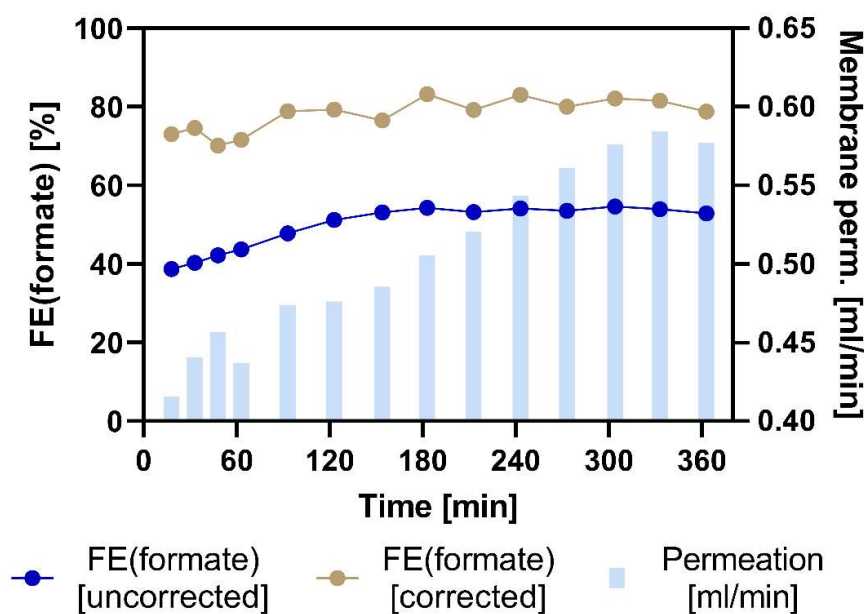# Section 8a: FE(formate) vs time corresponding Figure 7A & 7B

Figure S15 FE(formate) and membrane permeation vs time (corresponding with a high permeating membrane: Figure 7A in main article). The high membrane permeation was achieved by utilizing a thin N211 membrane. Catalyst used is SnO$_2$ nanoparticles.
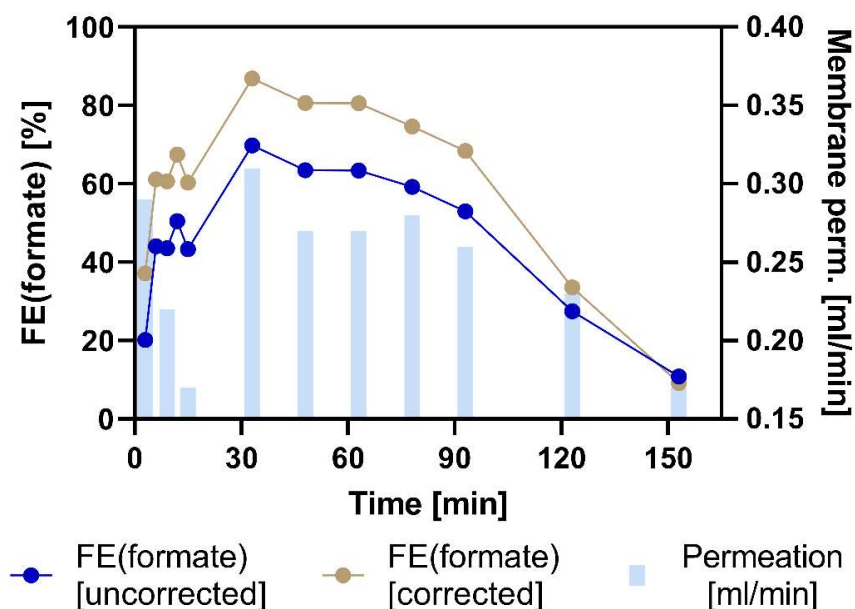

Figure S16 FE(formate) and membrane permeation vs time (corresponding with a low permeating membrane: Figure 7B in main article). The low membrane permeation was achieved by utilizing a N117 membrane. Catalyst used is SnO$_2$ nanoparticles.

Section 8b: EDS-spectra corresponding Figure 7A & 7B

Figure S17 EDS spectrum of a GDE-supported SnO$_2$ catalyst layer that was employed under high membrane permeating conditions (corresponding to Figure 7A in the main article). Energy dispersive spectroscopy (EDS) measurements were performed using a Super-X detector on the FEI quanta FEG250 at an acceleration voltage of 25 kV.
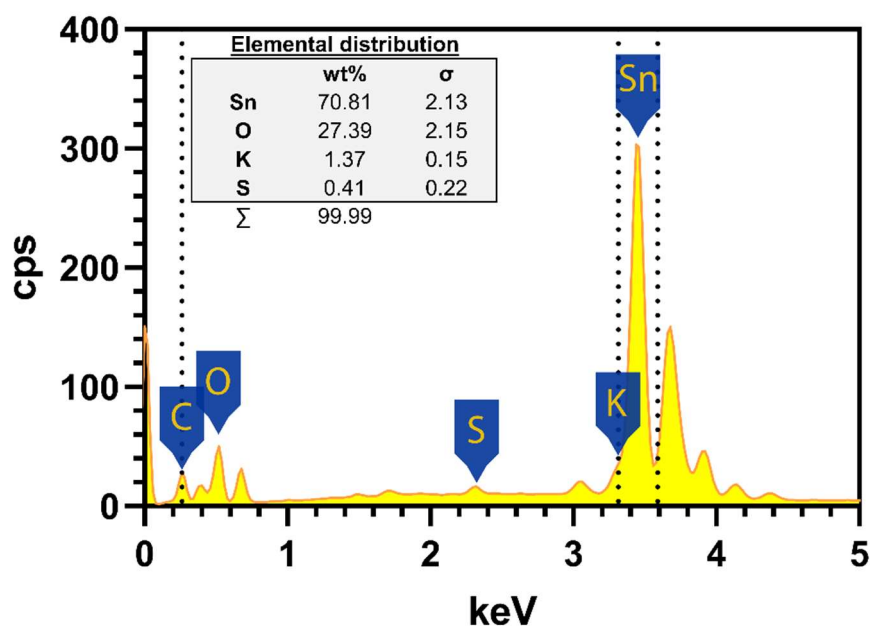

Figure S18 EDS spectrum of a GDE-supported SnO$_2$ catalyst layer that was employed under low membrane permeating conditions (corresponding to Figure 7B in the main article). Energy dispersive spectroscopy (EDS) measurements were performed using a Super-X detector on the FEI quanta FEG250 at an acceleration voltage of 25 kV.
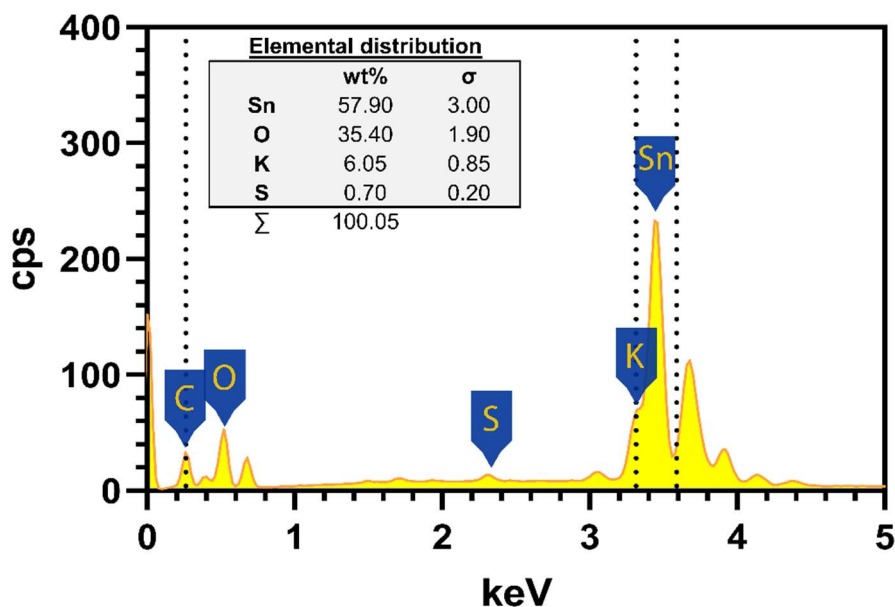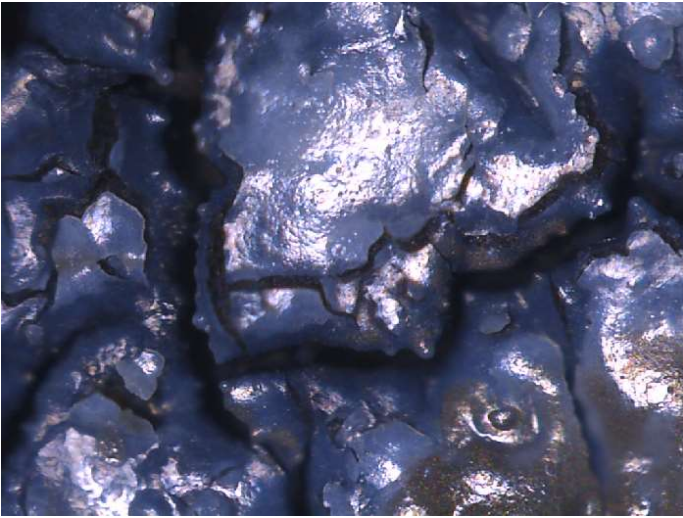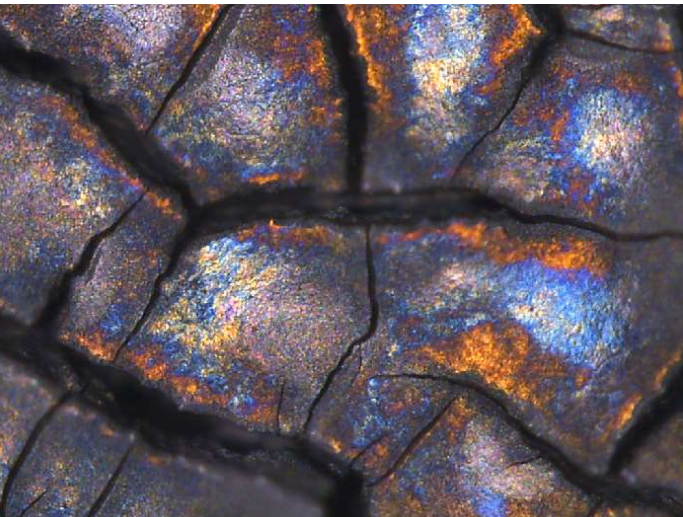
Section 9: Microscopic images of GDE's used under low and high membrane permeation condition

Low membrane permeation (0.23 ± 0.04 ml/min) for 2.5 hours	*Figure S19 Microscopic image (magnification x6.3) of catalyst layer (SnO$_2$) of a GDE used under low membrane permeation conditions (0.23 ± 0.04 ml/min) for 2.5 hours at 100 mA/cm². The catalyst layer is covered by a significant salt layer.*
High membrane permeation (0.52 ± 0.05 ml/min) for 6 hours	*Figure S20 Microscopic image (magnification x5.0) of catalyst layer (SnO$_2$) of a GDE used under high membrane permeation conditions (0.52 ± 0.05 ml/min) for 6 hours at 100 mA/cm².*

Section 10: Performance of pristine N117 membranes from different production batches
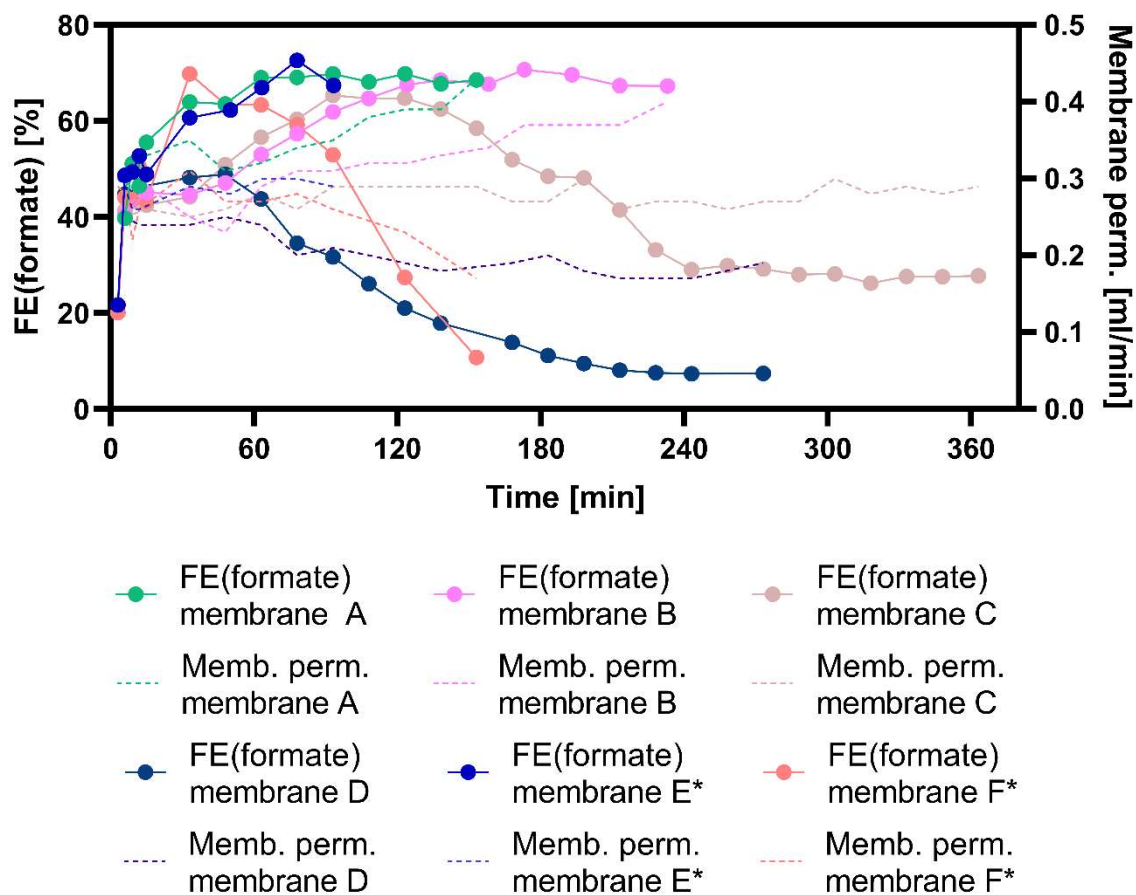

Figure S21 FE(formate, uncorrected) and membrane permeation rate vs time for six pristine N117 membranes from different production batches, operated under identical operating conditions (100 mA/cm²) with SnO₂ as cathode catalyst.

Section 11: Membrane activation procedure

Prior to the initial use of a Nafion membrane (both N117 & N211), a membrane activation protocol comprising four steps is carried out:

1. Boiling for one hour in a 3 vol% hydrogen peroxide (H_2O_2) solution with continuous refluxing. ➔ Removal of impurities in the membrane.

2. Boiling for one hour in ultrapure water. ➔ Removal of hydrogen peroxide traces and hydration of the membrane.

3. Boiling for one hour in a 0.75 M sulfuric acid (H_2SO_4) solution with continuous refluxing. ➔ Protonation of functional groups inside the membrane.

4. Boiling for one hour in ultrapure water. ➔ Removal of sulfuric acid traces and hydration of the membrane.

After the activation procedure, the membrane is stored in an ultrapure water container placed in a refrigerator (T = 4°C). This container is closed-off from the atmosphere to prevent contamination.

Section 12: Membrane degradation N117 membrane
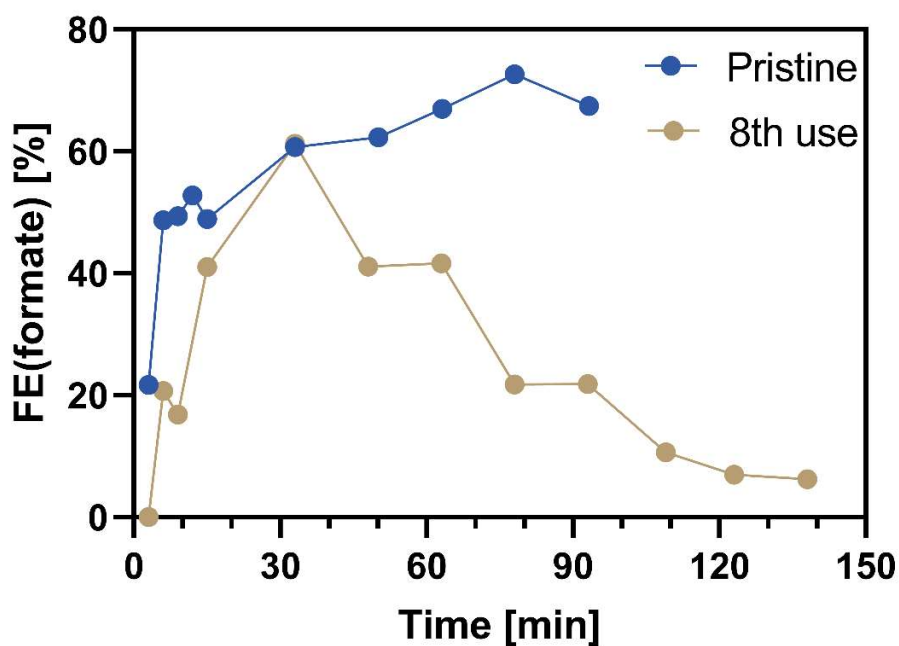
Figure S22 Influence of reusing membrane on FE(formate) stability. Blue curve shows performance for a pristine N117 membrane, while brown curve represents the FE for the same membrane after eight identical experimental runs (120 min) with intermittent storage in ultrapure water.
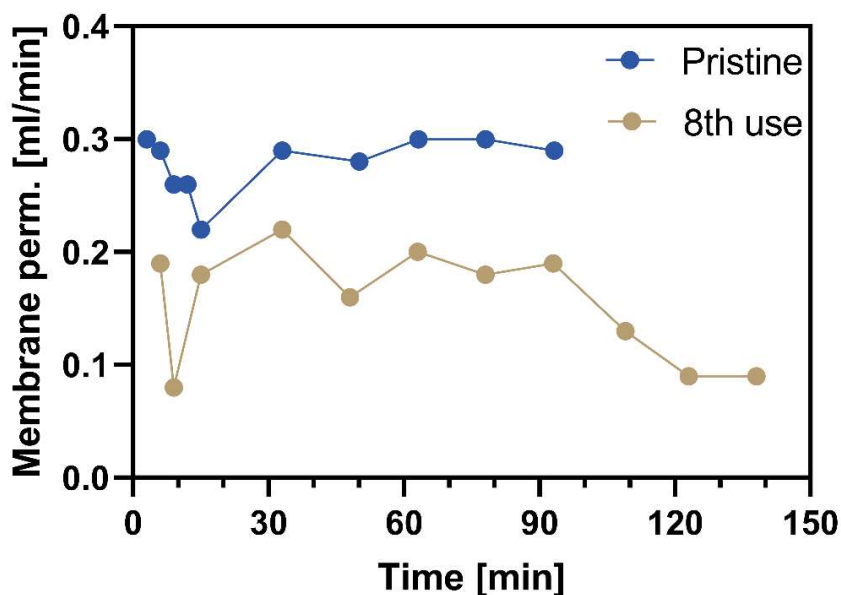
Figure S23 Influence of repeated membrane use on membrane permeation rate. The blue curve shows permeation through a pristine N117 membrane, while the brown curve represents the permeation through the same membrane after eight runs with intermittent storage in ultrapure water.

Figure S24 Influence of repeated membrane use on cell voltage. The blue curve shows the cell voltage profile for a pristine N117 membrane, while the brown curve represents the cell voltage with the same membrane after eight runs with intermittent storage in ultrapure water.

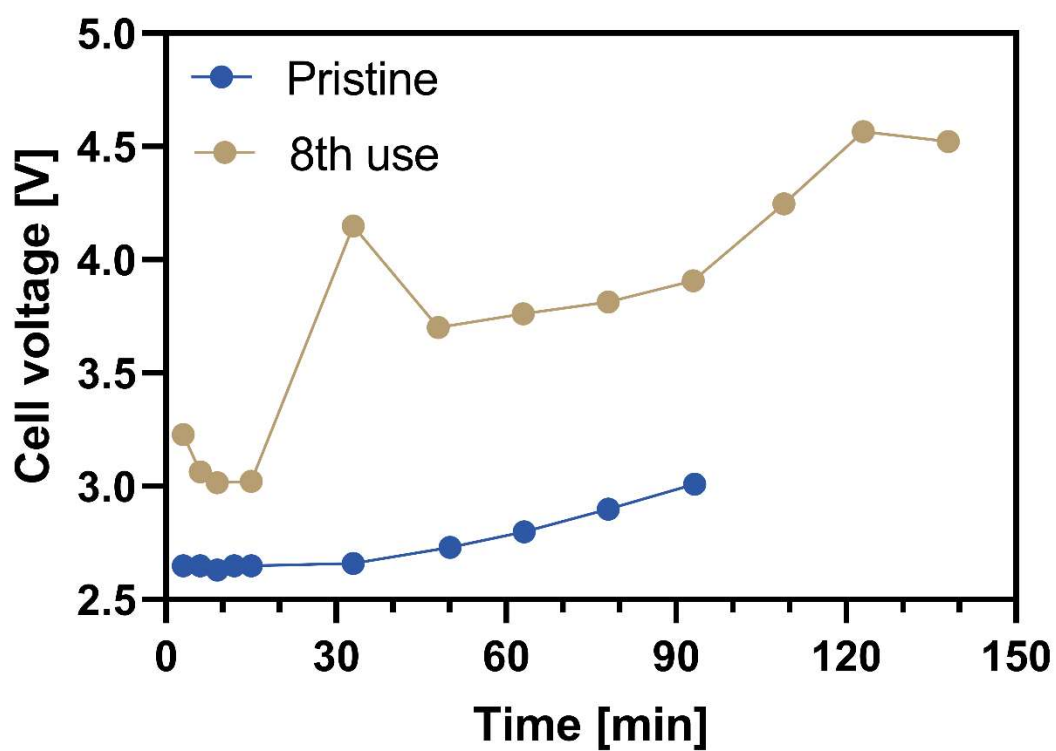# Section 13: Impedance study on N117 membranes

Intrinsic differences between pristine membranes
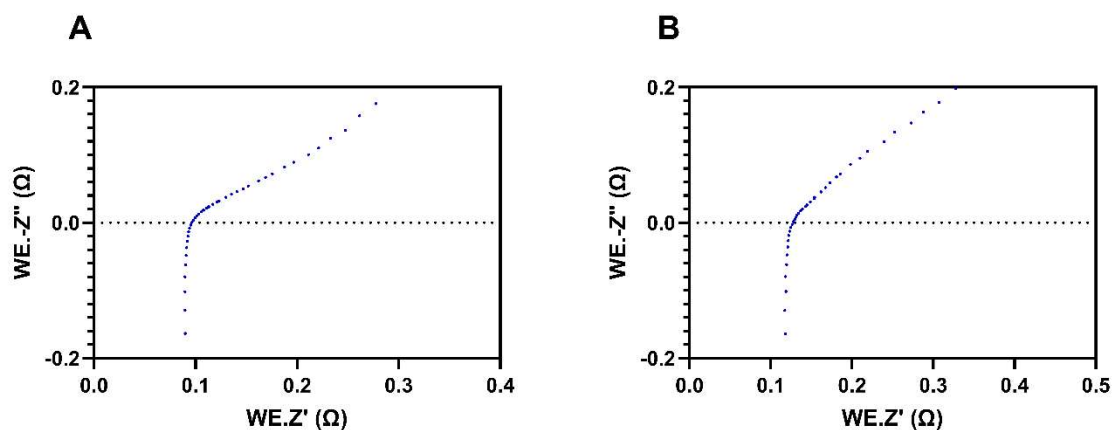
Figure S25 Electrochemical impedance spectroscopy (EIS) measurements at open circuit voltage (OCV) expressed as Nyquist plots for two pristine membranes: membrane A high membrane permeation ($0.32 \pm 0.02\ ml/min$) and membrane B low membrane permeation (0.23 ± 0.02). Both EIS measurements are performed after an initital linear sweep of cell voltage between 2.2 and 3.0 V to activate the membranes. These results were achieved by utilizing the same cell as in the galvanostatic experiments (ESI Section 1).

Table S1 Summary ohmic resistances (average and standard deviation of two/three measurements) visualized in Figure S25.

	R [Ω]		R [$\Omega \cdot cm^2$]	
	$\overline{x}$	St. Dev	$\overline{x}$	St. Dev
A	0.100	0.003	4.9	0.2
B	0.126	0.002	6.2	0.1

Membrane degradation
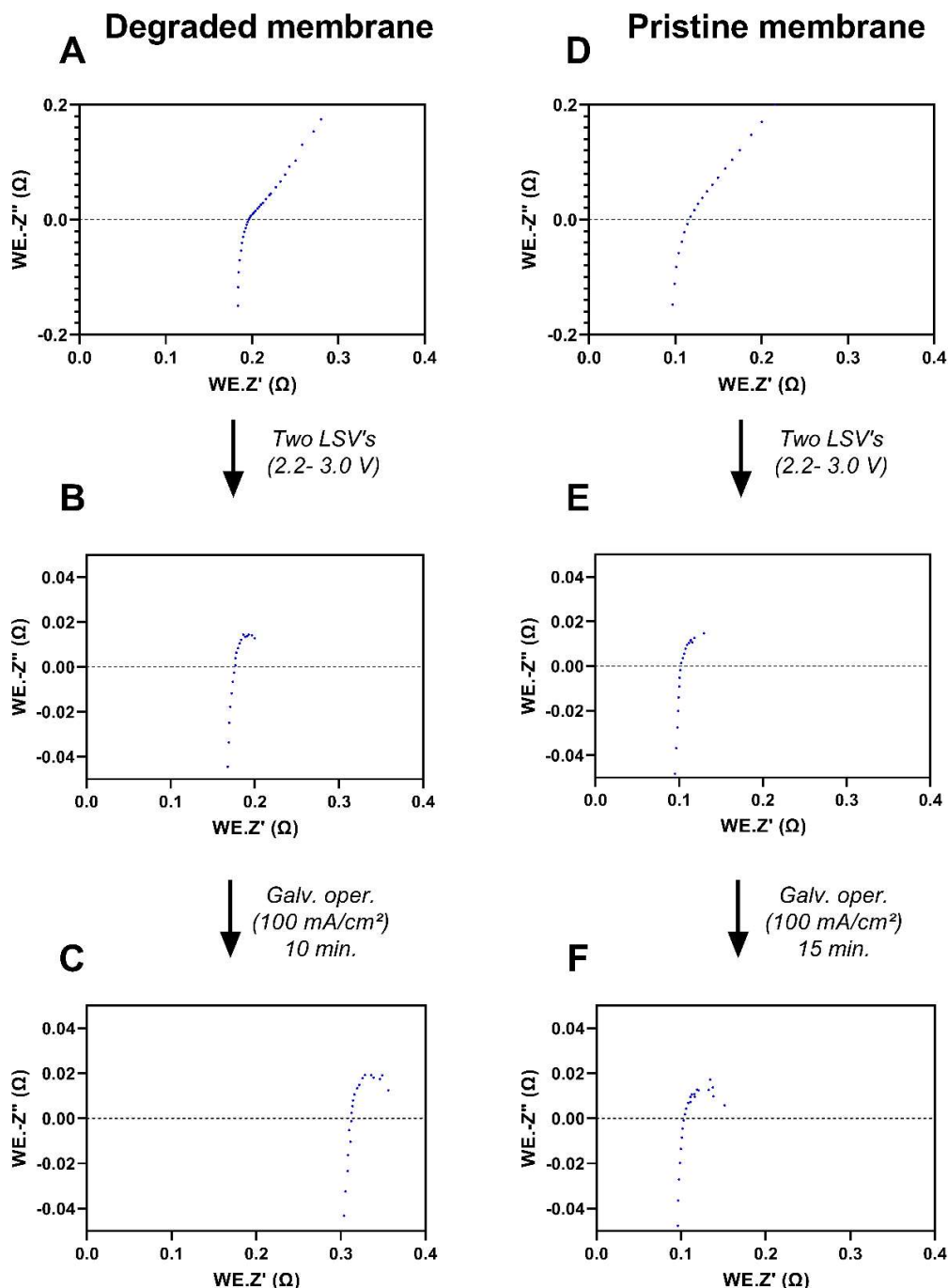
Figure S26 Electrochemical impedance spectroscopy (EIS) results expressed as Nyquist plots for a degraded membrane (A-C) and a pristine membrane (D-F) at three stages. A) EIS at OCV on a degraded membrane just after assembly, B) EIS at 3 V on a degraded membrane after two LSV's (2.2 - 3.0 V), C) EIS at 3 V on a degraded membrane after 10 minutes of galvanostatic operation (100 mA/cm²), D) EIS at OCV on a pristine membrane just after assembly, E) EIS at 3 V on a pristine membrane after two LSV's (2.2 – 3.0 V), F) EIS at 3 V on a pristine membrane after 15 minutes of galvanostatic operation (100 mA/cm²). These results were achieved by utilizing the same cell as in the galvanostatic experiments (ESI Section 1).

Table S2 Summary ohmic resistances (average and standard deviation of two/three measurements) visualized in Figure S26.

	R $[\Omega]$		R $[\Omega \cdot cm^2]$	
	$\overline{x}$	St. Dev	$\overline{x}$	St. Dev
A	0.193	0.005	9.46	0.25
B	0.176	0.002	8.60	0.10
C	0.318	0.008	15.56	0.38
D	0.116	0.001	5.70	0.02
E	0.102	0.001	5.01	0.03
F	0.104	0.001	5.11	0.06

Section 14: IR-absorption bands of N117 membranes
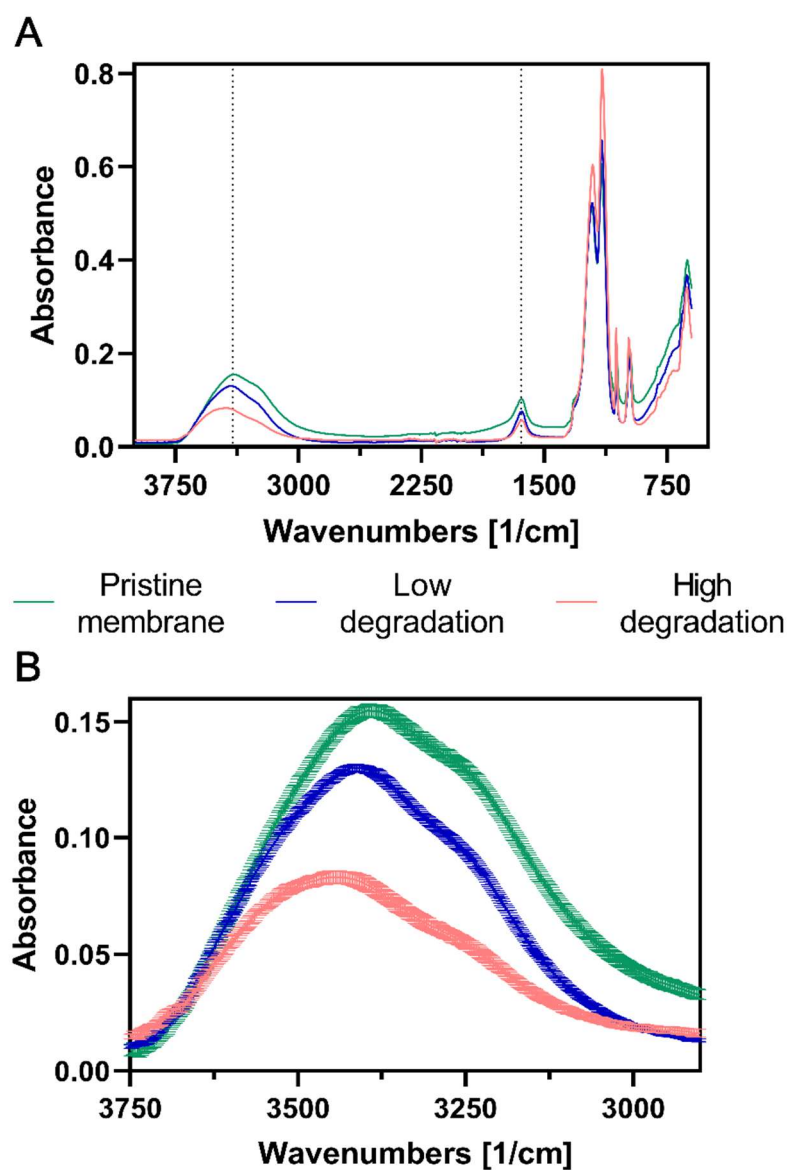
Figure S27 (A) Infrared spectroscopy spectra of N117 membranes. Scan range 600 - 4000 cm^{-1}. The absorption bands at 1640 & 3400 cm^{-1} are attributed to the presence of water in the structure.[4] The green curve corresponds to a pristine membrane; the blue curve to a membrane that was used four times; the red curve to a membrane used 15 times. Figure B is a close-up of the 3400 cm^{-1} absorption peaks in figure A with error flags (4 IR-scans).

The membrane hydration state is governed by the amount of water incorporated in the Nafion structure, which can be assessed by the intensity of water absorption peaks (1640 & 3400 cm^{-1}) in Figure S27.[4]

Section 15: Electrolyzer performance with optimal settings

By optimizing the reactor conditions based on the findings in this study (see Table S3), we were able to achieve a stable, high FE(formate) of 95.2 ± 2.3 % for six hours, visualized in Figure S28, or 96.7 ± 0.8 % when excluding formate re-oxidation events.

Figure S28 FE(formate) vs time for the electrolyzer with optimal operating conditions: Bi₂O₃ as cathode catalyst and N211 membrane for high permeation rates.

Table S3 Overview process conditions and performance for Figure S28.

Catalyst	Bismuth oxide (Bi_2O_3)
Catalyst loading	$4.00 \pm 0.02 \, mg/cm^2$
Current (density)	4.9 A (100 mA/cm^2)
Cell voltage	$2.49 \pm 0.12 \, V$
Membrane permeation	$0.53 \pm 0.04 \, ml/min$

Salt crystallization	< 1 mg/cm^2
FE(HCOO$^-$, uncorrected)	45.7 ± 2.3 %
FE(HCOO$^-$, corrected)	96.7 ± 0.8 %
Recovery Rate	46.1 ± 2.7 %
Cathode concentration	51.4 ± 4.5 g/l HCOOK
Anode (final) concentration	28.3 ± 1.2 g/l HCOOK

Figure S29 Cell voltage vs time for the electrolyzer with optimal operating conditions: Bi$_2$O$_3$ as cathode catalyst and N211 membrane for high permeation rates.
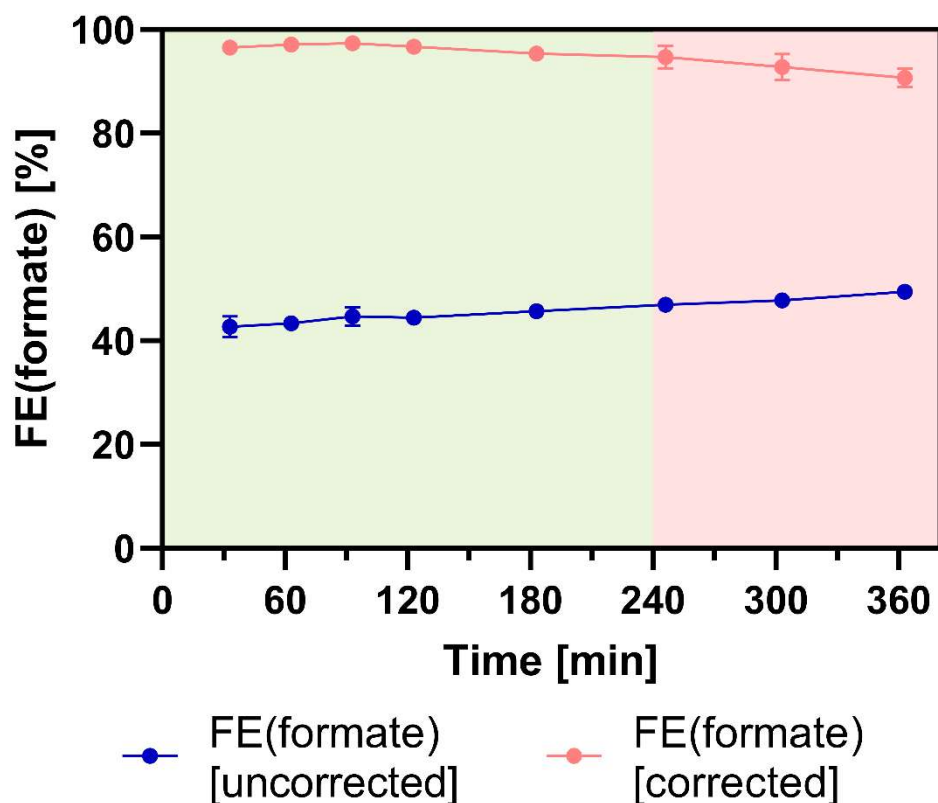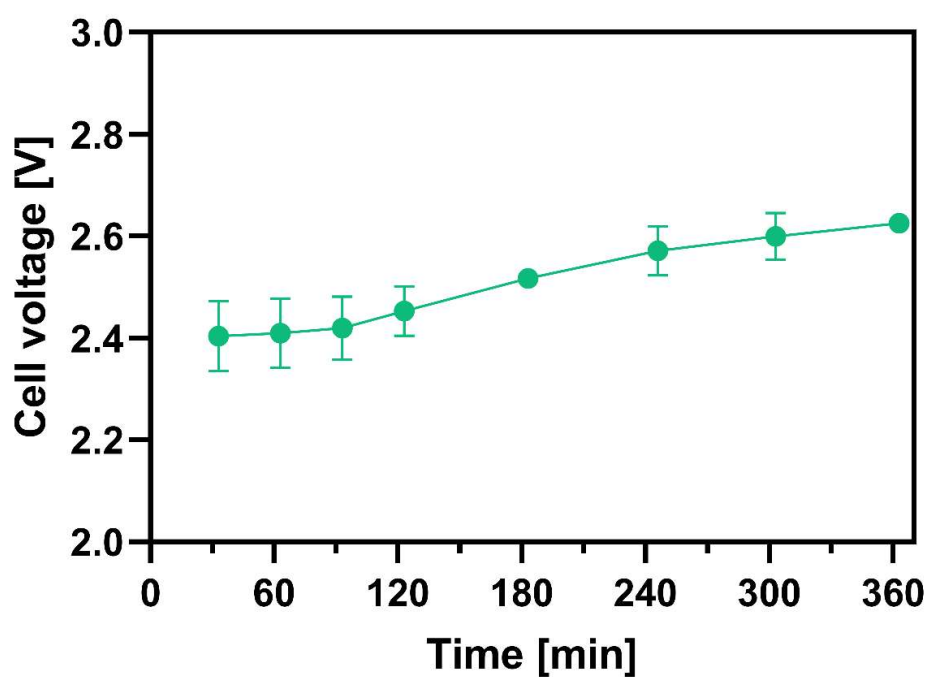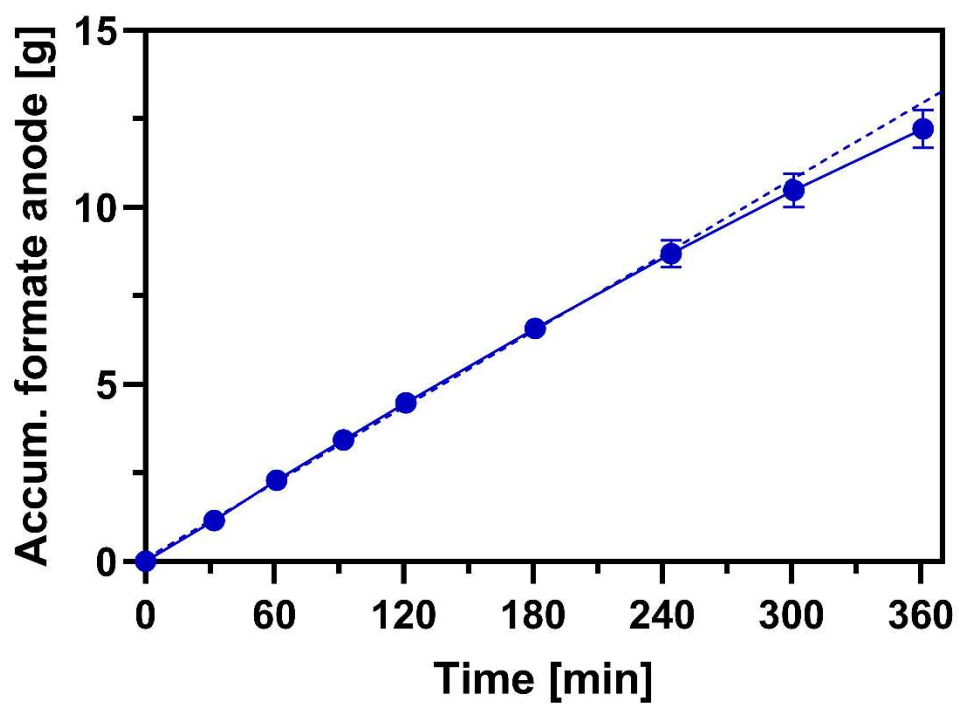
Figure S30 Accumulated mass of formate in anolyte vs time for the electrolyzer with optimal operating conditions: Bi_2O_3 as cathode catalyst and N211 membrane for high permeation rates.

Section 16: Sigracet 39AA GDE

Since the DWI supply is not able to reach the cathode catalyst layer at a sufficient rate to remove the produced salts, optimization of the GDE design proves to be a promising approach to increase process controllability. As a proof of concept, a control experiment was performed where a Sigracet 39AA was utilized as cathode GDE. This electrode has similar properties to the 39BB GDE discussed in this work, but is manufactured without MPL-layer and PTFE treatment. The GDE was manually treated to have a 10-15 wt.% (PTFE-based) Nafion content at its GDE-membrane interface by spray coating. The cathode was supplied with 0.65 ml/min DWI-feed and 0.26 ± 0.03 ml/min MP. The lack in hydrophobicity however resulted in a low CO_2 conversion with an FE of 8.31 ± 0.88 %, as visualised in Figure S31.
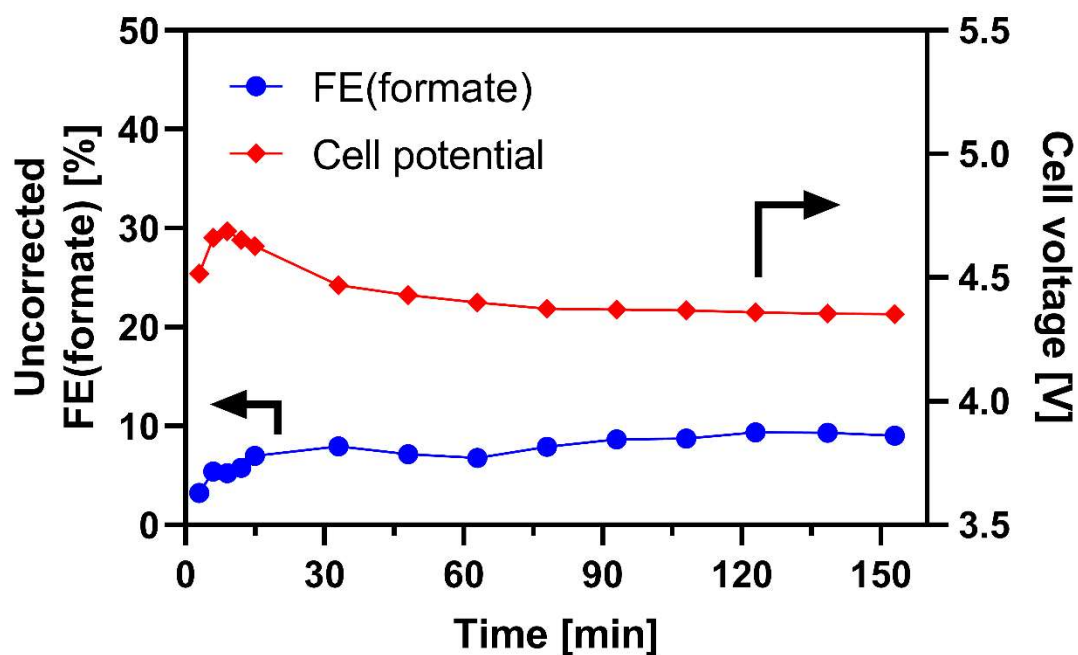
Figure S31 Uncorrected FE(formate) and cell voltage vs time for a 39AA GDE with 4.02 mg/cm² SnO₂ catalyst.

Section 17 – Reversing membrane degradation

Due to changes in hydration state of the membrane, a degradation of the membrane performance was observed resulting in a decreasing membrane permeation when reusing in time. To recover the pristine membrane performance, a re-activation was attempted following the identical procedure as discussed in ESI – Section 11.

As visualized in Figure S33, by reactivating the membrane a significant improvement in MP (blue bars to red bars) and CO2RR stability (blue curve to red curve) is observed, however insufficient to regain pristine performance (orange curve and bars).

Figure S32 Effect of re-activating N117 membrane after significant degradation on the CO2RR stability and MP.

Section 18 – Additional discussion

<u>What is the influence of cation specie on water management?</u>

As discussed in the manuscript on p.7, smaller cations exhibit a higher hydration state, resulting in enhanced water management through the membrane. Therefore, an interesting approach to improve water management is usin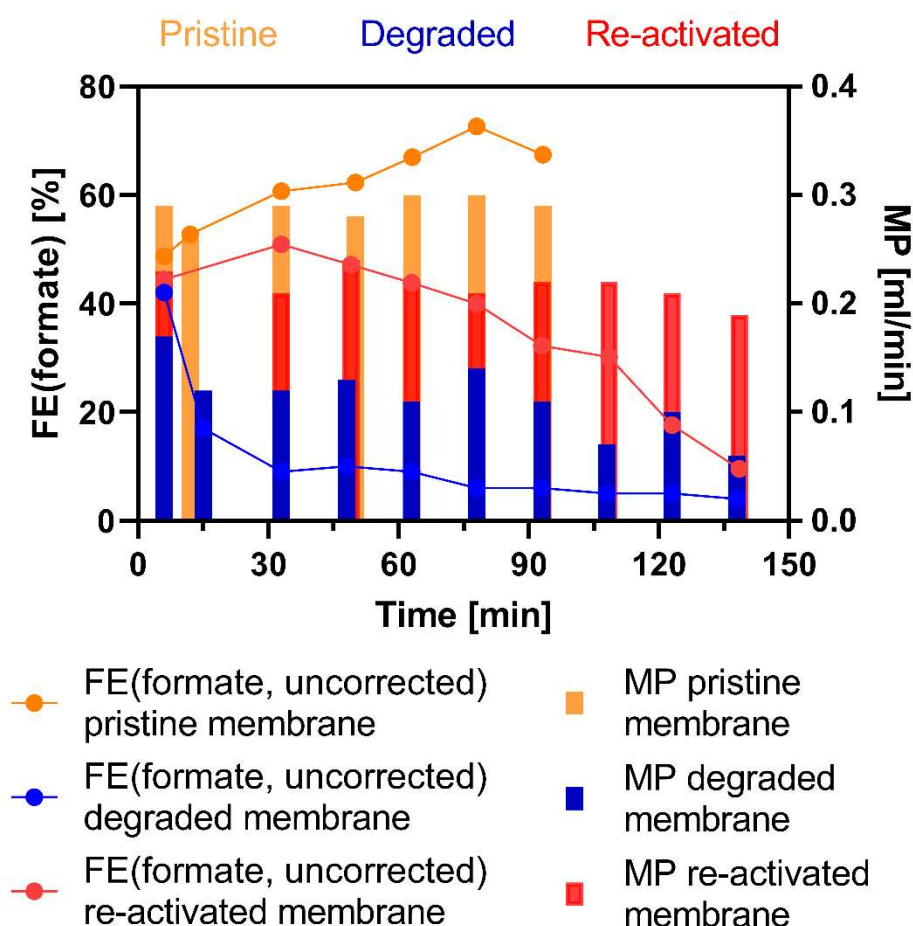g smaller cation species as charge transfer species, e.g. Li^+ or Na^+, to increase the membrane permeation rate, allowing for the use of a thicker ion exchange membrane to minimize the formate crossover.

In this work, however, we solely focused on the potassium cation as charge transport specie due to its distinct contribution in the CO2RR mechanism.[5] From literature it is known that the use of smaller cations (Li^+ and Na^+) lower the efficiency towards C-products and promotes the HER.[6], [7] Importantly, we also rationalized that the use of smaller cations as charge transport specie would result in significantly lower salt solubilities in the cathode, thus exacerbating the cathode salt management issues: Li_2CO_3 [1.3 g/100 ml] < Na_2CO_3 [30.7 g/100 ml] < K_2CO_3 [111.4 g/100 ml] at 25°C.[8]

When using Cs^+ cations as charge transfer specie, we assume that membrane permeation will be lower due to the lower cation hydration number. While this is disadvantageous for the cathode water management, the Cs^+ as charge transport specie would result in the formation of highly soluble Cs-carbonate salts (Cs_2CO_3 [261 g/100 ml] vs K_2CO_3 [111.4 g/100 ml] at 25°C), facilitating the salt removal through the cathode product.[9] However, the high price tag of CsOH vs KOH, 1230 euro/kg [Fischer Scientific][10] vs 44 euro/kg [VWR][11], makes it unsuitable for industrial application.

What is the influence of anolyte volume on the process?

When increasing the anolyte volume, effects could be observed in i) cell voltage, ii) anode formate concentration, iii) formate re-oxidation. Firstly, when a higher (initial) volume of anolyte is used, a slower depletion of KOH could be expected (galvanostatic operation) and therefore a slower decrease in conductivity/increase in resistance. This would result in a more stable cell voltage. Secondly, in a higher volume of anolyte, for the same rate of formate crossover, a slower increase in formate concentration would be expected. Lastly, assuming the anode formate concentration influences the onset of the formate re-oxidation would imply the re-oxidation can be postponed by operating with a higher anolyte volume. The influence of formate concentration on the re-oxidation however needs further attention in future work focusing on the anode oxidation reaction.

What is the influence of anolyte concentration on the process?

In three ways: i) cell voltage, ii) membrane charge selectivity, and iii) membrane permeation.

When utilizing an anolyte with a higher $C(KOH)$, a higher conductivity of the anolyte and therefore a lower cell voltage could be expected. When increasing the anolyte concentration, and therefore the presence of K^+ at the anolyte-membrane interface, a higher flux of K^+ through the membrane is expected, hence influencing the total charge balance as visualized in Figure 3 of the manuscript. In the experiments within this study, a concentration of 1.7 M was opted to be able to run continuously for +6 hours while preventing significant anolyte mass-transfer limitations, allowing the investigation of the cathode stability. Lastly, the MP can also be influenced by the anolyte concentration. While the driving forces for the water transport from anode to cathode within zero-gap electrolyzers are not yet fully understood, we assume osmotic pressures plays an important role. When the anolyte concentration is lowered, a

decrease in osmotic pressure would result in an increase in the net MP from anode to cathode, benefiting cathode salt management. However, this needs to be studied in detail in future work.

What is the effect operating the anolyte single-pass instead of recirculation?

This would result in similar observations as expected when working with a higher anolyte volume. Especially the formate concentration in the anolyte would significantly be reduced, lowering the economical value of formate in the anolyte. This is a result of the high anolyte flowrate utilized in the anode compartment to remove the formed oxygen bubbles swiftly to prevent fluctuations in cell voltage. To prevent very high volumes of anolyte (and costs) in our up-scaled electrolyzer, we opted for recirculation.

What was the visual effect of membrane degradation on the appearance of the membrane?

When the N117 degraded, resulting in a lowering of the membrane permeation, a shrinking of the membrane dimensions (up to 7%) was observed, followed by a significant tension on the membrane when disassembling the electrolyzer after use. This shrinking phenomenon was not resolved by placing the membrane in water in between experiments. We explain in the manuscript that dehydration of the membrane - due to the harsh conditions on the cathode-membrane interface - reduces the pore sizes of the Nafion structure and therefore also membrane dimensions.

What phase is the DWI-supply introduced into the cathode compartment?

In the zero-gap electrolyzer we consider two possible pathways for water towards the cathode: i) membrane permeation and ii) water injection with CO_2 through the GDE. Our present work focuses on the former due to the observation that the DWI water is not able to reach the catalyst surface sufficiently. In future work we plan to shift our focus from the membrane to the GDE and optimize the second pathway, to reduce the

role of the membrane and improve the general process' controllability. The temperature of the CO_2/water will be one aspect which will be studied. We assume that when the water is supplied in the form of water vapor, the water will reach the catalyst surface more easily. However, to dissolve and remove the formed carbonate salts, that water has to be present in liquid form, implying that condensation has to occur inside the cathode compartment. However, at high CD operation, the temperature of the electrode surface will rise, possibly with enhanced evaporation as a result. As calculated in ESI – Section 5.3, at room temperature (298 K), a saturated gas will contain 0.014 ml/min water vapor, but this value increases rapidly with temperature. At 50°C, the saturated CO_2 will contain 0.058 ml/min water and 0.237 ml/min at 75°C, depicted in the figure below. To supply the minimum water amount of 0.3 ml/min (at 100 mA/cm² and 49 cm²) a minimum inlet temperature of 78.5°C is required. However this assumes that all the water vapor condenses at the catalytic active area, which is unlikely. Therefore the CO_2/water mixture should be supplied at a higher temperature than 78.5°C, assuming an electrode at standard temperature.
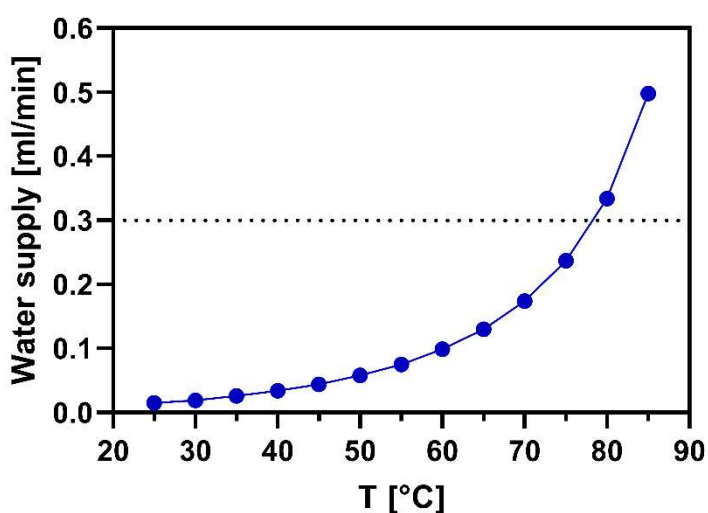

Figure S33 Influence of temperature on water vapor supply

One of the main strengths of electrolytic processes is the possibility to work at room temperature and therefore no pre-heating of CO_2 was opted in this study.

Nickel foam stability in the anode compartment

After multiple reuses of the nickel foam, a color change could be observed, transitioning from its initial light grey to a darker grey with darker spots. As the primary focus of this work is on the stability of the cathode compartment, with the anode serving solely as an electron donor, no additional analyses were conducted on the anode catalyst. If the nickel foam underwent significant visual changes, a new nickel foam was employed for subsequent experiments.

Since in the zero-gap electrolyzer no reference electrode is present, changes relating the anode catalyst are difficult to detect since a rise in cell voltage can be the result of multiple causes.

Author Information

Corresponding Authors

Lieven Hintjens - Applied Electrochemistry and Catalysis (ELCAT), University of Antwerp, 2610 Wilrijk, Belgium.

https://orcid.org/0000-0001-8444-1919

Email: Lieven.hintjens@uantwerpen.be

Sam Van Daele - Applied Electrochemistry and Catalysis (ELCAT), University of Antwerp, 2610 Wilrijk, Belgium.

https://orcid.org/0000-0002-4805-9170

Email: sam.vandaele@uantwerpen.be

Jonathan Schalck - Applied Electrochemistry and Catalysis (ELCAT), University of Antwerp, 2610 Wilrijk, Belgium.

https://orcid.org/0000-0003-4118-0266

Email: jonathan.schalck@uantwerpen.be

Michiel Vranckaert - Applied Electrochemistry and Catalysis (ELCAT), University of Antwerp, 2610 Wilrijk, Belgium.

https://orcid.org/0009-0007-1836-3861

Email: michiel.vranckaert@uantwerpen.be

Sander Neukermans - Applied Electrochemistry and Catalysis (ELCAT), University of Antwerp, 2610 Wilrijk, Belgium.

https://orcid.org/0000-0003-1672-2481

Email: sanderneukermans@gmail.com

Daniel Choukroun - Applied Electrochemistry and Catalysis (ELCAT), University of Antwerp, 2610 Wilrijk, Belgium.

orcid.org/0000-0002-3047-2506

Email: Daniel.Choukroun@uantwerpen.be

Tom Breugelmans - Applied Electrochemistry and Catalysis (ELCAT), University of Antwerp, 2610 Wilrijk, Belgium.

orcid.org/0000-0001-5538-0408

Email: tom.breugelmans@uantwerpen.be

Author Contributions

Lieven Hintjens: Writing – Original Draft, Conceptualization, Investigation. **Sam Van Daele**: Writing – review & editing, Conceptualization. **Jonathan Schalck**: Writing – review & editing, Conceptualization. **Michiel Vranckaert**: Writing– review & editing, Investigation. **Sander Neukermans**: Writing – review & editing, Conceptualization, Supervision. **Daniel Choukroun**: Writing – review & editing, Conceptualization, Supervision. **Tom Breugelmans**: Writing – review & editing, Project administration, Funding acquisition.

Acknowledgement

References

[1]   S. Van Daele *et al.*, "Influence of the target product on the electrochemical reduction of diluted CO2 in a continuous flow cell," *J. CO2 Util.*, vol. 65, p. 102210, Nov. 2022, doi: 10.1016/J.JCOU.2022.102210.

[2]   K. Yang and M. Qin, "The application of cation exchange membranes in electrochemical systems for ammonia recovery from wastewater," *Membranes*, vol. 11, no. 7. MDPI AG, Jul. 01, 2021. doi: 10.3390/membranes11070494.

[3]   W.M. Haynes; David R. Linde; Thomas J. Bruno, *CRC Handbook of Chemistry and Physics*, 95th ed., vol. 6. Florida: CRC Press, 2015.

[4]   Y. Weiss, I. Kiflawi, and O. Navon, "The IR absorption spectrum of water in microinclusions-bearing diamonds."

[5]   C. Ye, F. Dattila, X. Chen, N. López, and M. T. M. Koper, "Influence of Cations on HCOOH and CO Formation during CO2 Reduction on a PdMLPt(111) Electrode," *J. Am. Chem. Soc.*, vol.

145, no. 36, pp. 19601–19610, Sep. 2023, doi: 10.1021/jacs.3c03786.

[6]   M. C. O. Monteiro, F. Dattila, B. Hagedoorn, R. García-Muelas, N.

       López, and M. T. M. Koper, "Absence of CO2 electroreduction on

       copper, gold and silver electrodes without metal cations in

       solution," *Nat. Catal.*, vol. 4, no. 8, pp. 654–662, Aug. 2021, doi:

       10.1038/s41929-021-00655-5.

[7]   B. Pan, Y. Wang, and Y. Li, "Understanding and leveraging the

       effect of cations in the electrical double layer for electrochemical

       CO2 reduction," *Chem Catalysis*, vol. 2, no. 6. Cell Press, pp. 1267–

       1276, Jun. 16, 2022. doi: 10.1016/j.checat.2022.03.012.

[8]   W.M. Haynes; David R. Linde; Thomas J. Bruno, *CRC Handbook

       of Chemistry and Physics*, 95th ed., vol. 5. Florida: CRC Press,

       2015.

[9]   M. Sassenburg, M. Kelly, S. Subramanian, W. A. Smith, and T.

       Burdyny, "Zero-Gap Electrochemical CO2 Reduction Cells:

       Challenges and Operational Strategies for Prevention of Salt

       Precipitation," *ACS Energy Lett.*, vol. 8, no. 1, pp. 321–331, Jan.

2023, doi: 10.1021/acsenergylett.2c01885.

[10] "https://www.fishersci.be/shop/products/cesium-hydroxide-monohydrate-96-cesium-carbonate-5-thermo-scientific/11490657."

[11] "https://be.vwr.com/store/product/nl/2376844/kaliumhydroxide-pellets-emsure-acs-reag-ph-eur-for-analysis-max-0-05-na-supelco."